



Strangeness production in double gap events in ALICE

R. Schicker¹

(on behalf of the ALICE collaboration)

¹Physikalisches Institut, Im Neuenheimer Feld 226, Heidelberg, Germany

December 5, 2023

Abstract

The ALICE detector at the LHC was upgraded in the long shutdown of 2019-2021 in order to take data at much-increased Run 3 and 4 rates. The various challenges of this upgrade are presented, and the first results of strangeness production in double gap events collected in 2022 are shown by presenting distributions of kaon pairs.

1 Introduction

In the long shutdown of 2019-2021, the ALICE experiment was upgraded in order to take data at much-increased rates in Runs 3 and 4 [1]. The readout was changed to continuous mode, with the data collected in proton-proton collisions at a typically 1 MHz rate and subsequently being processed to identify the events of interest. The selected events are permanently stored for future processing. All data taken in heavy-ion collisions at up to 50 kHz are permanently stored, and available for later analysis.

2 The ALICE detector upgrades

The Time-Projection-Chamber (TPC) is not only the main tracking detector of the ALICE experiment but also provides information on the specific ionisation loss dE/dx for particle identification. The ionisation electrons drift in the electric field of 400 V/cm to the endplates of the cylindrical field cage. The ionisation charge was amplified in Runs 1,2 by multiwire proportional chambers (MWPCs), with the backflow of positive ions being controlled by gating grids. The effective rate was limited in Runs 1,2 to ~ 1 kHz. In order to increase the rate capability to ~ 50 kHz, the MWPCs were replaced by a stack of 4 Gas Electron Multipliers (GEMs) with continuous readout and synchronous data processing [2].

The readout rate of the Inner Tracking System (ITS) in Runs 1,2 was limited to 1 kHz. The Run 3 newly designed system features improved resolution, less material and faster readout. The new system consists of 7 layers of Monolithic Active Pixel Sensors, with a spatial resolution ($r\phi \times z$) improved from 11×100 (μm^2) of the old ITS to 5×5 (μm^2). The readout rate of this new ITS system is 100 kHz in Pb-Pb, and 200 kHz in pp collisions [3].

Outside of the central barrel pseudorapidity range $|\eta| < 0.9$, a Fast Interaction Trigger (FIT) system was built for Run 3 to provide precise collision time information for time-of-flight-based particle information, for online luminosity monitoring and measuring forward multiplicity [4]. This FIT system consists of the following detectors:

- **FT0:** Two Cherenkov arrays for minimum bias triggering, for determining the collision time and for vertex position calculation.
- **FV0:** A large scintillator array consisting of five rings and eight sectors is positioned on the opposite side of the ALICE muon spectrometer. In conjunction with FT0, it is used for centrality and event plane determination in heavy-ion collisions.
- **FDD** (Forward Diffractive Detector): This double-sided scintillator array is essential for tagging diffractive events by establishing rapidity gaps in the event.

Detector	η_{min}	η_{max}	z [cm]
FDD-A	4.8	6.3	1696.0
FT0-A	3.5	4.9	334.6
FV0	2.2	5.1	320.8
FT0-C	-3.3	-2.1	-84.3
FDD-C	-7.0	-4.9	-1956.6

Table 1: The pseudorapidity range and the z-position of the FIT subsystems.

The parameters of the different subsystems of the FIT detector are shown in Table 1.

3 The computing system upgrade

After the upgrade of the ALICE detector systems in the long shutdown of 2019-2021, the raw data flow to the data acquisition system increased a hundredfold, up to 3.5 TB/s. A new Online/Offline Computing system, O², was developed to cope with this challenge [5]. The O² system incorporates continuous readout of most subdetectors, data compression using partial synchronous reconstruction and calibration, and the sharing of common computing resources during and, for asynchronous reconstruction, after data taking. The reconstructed data are written to disk while the raw data are discarded. The O² architecture consists of two major computing layers, the First Level Processors (FLPs) and the Event Processing Nodes (EPNs). Both layers are highly heterogeneous, with specialized acquisition cards embedding FPGAs on the FLPs, and GPUs on the EPNs. The raw data rate of 3.5 TB/s is reduced by the FLP layer to ~ 635 GB/s and by the EPN layer to 100 GB/s. This compressed data stream is stored and, after later asynchronous processing, distributed to the Tier 0 and Tier 1 analysis facilities.

This upgrade of the ALICE experiment resulted in a considerably increased data taking capability. The double gap data sample from Run 2 amounts to about 10 pb^{-1} . In Run 3, a central barrel data sample of $\sim 10 \text{ pb}^{-1}$ is recorded in 6 weeks.

4 Central diffractive production at the LHC

Central diffractive events are characterized by particle production at midrapidity and by the absence at forward and backward rapidities. The ALICE experiment is ideally suited for measuring such events due to the excellent global tracking in the central barrel by the combined information of TPC and ITS and the superb particle identification capability of the TPC. The absence of particle tracks at forward/backward rapidities can be established by requiring no signals in the FIT detector systems.

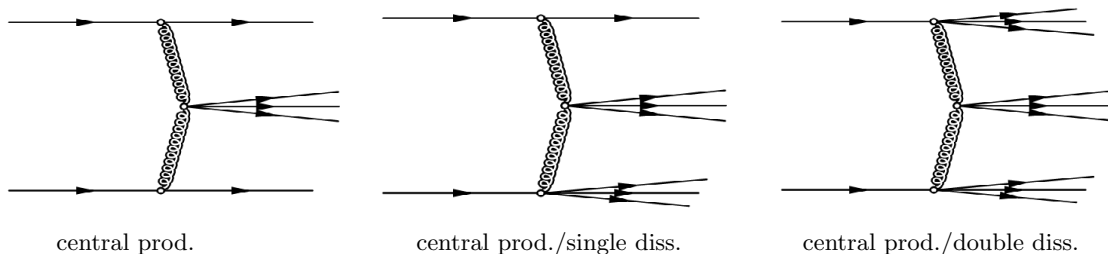


Figure 1: The event topologies of central production (left), central production with single dissociation (middle), and central production with double dissociation (right).

In Figure 1, the topologies of central production events are shown. In such events, one

or both protons can undergo a diffractive excitation, and subsequently break up into very forward scattered fragments. Central production at the energies of the LHC is dominated by the Pomeron-Pomeron exchange. In QCD, the Pomeron is thought to be a dominantly gluonic object. The study of particle yields in this gluonic environment, and the comparison to the corresponding yields in minimum bias collisions is of high interest in the search for QCD exotica such as hybrids and glueballs.

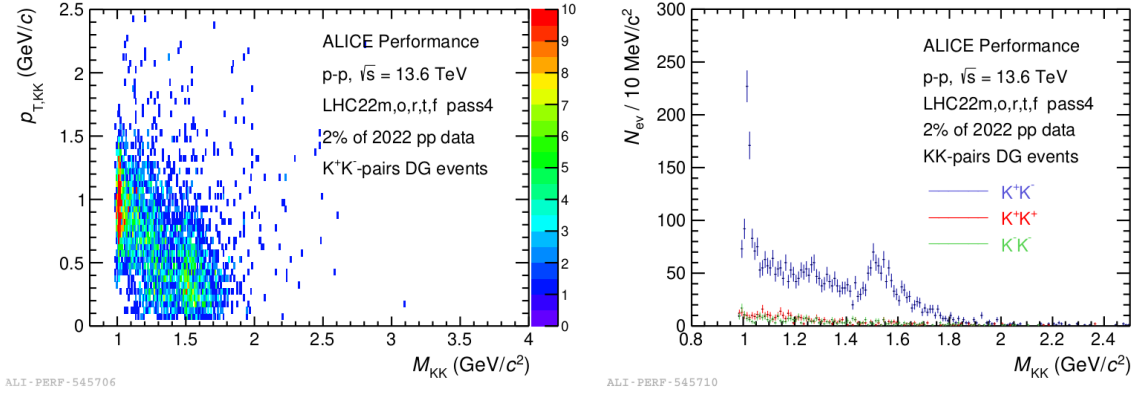


Figure 2: The mass of unlike-sign kaon pairs vs. pair transverse momentum (left), the mass distribution for like and unlike-sign kaon pairs (right).

In Fig. 2 on the left, the invariant mass of K^+K^- pairs in double gap events is shown as a function of pair transverse momentum. The mass distribution shown on the right is derived by integrating the 2-D distribution over transverse momentum. The mass distribution is shown for unlike and like-sign pairs, indicating contamination below the 10% level for the K^+K^- signal events. The data sample shown in Fig. 2 represents about 2% of the statistics taken in 2022.

Clearly visible in Fig. 2 on the right are peak structures just above the two kaon threshold, and at a mass $M_{KK} \approx 1.52 \text{ GeV}/c^2$. These two structures are tentatively identified as the $\phi(1020)$ and the $f'_2(1525)$, that has a known kaon branching ratio of 88%. The limited statistics analysed so far preclude the identification of further peaks. The ALICE data sample taken in 2022-2023 is larger by a factor of about 80 as compared to the sample shown in Fig. 2. The analysis of the full-data sample will hence be able to give much-improved information on the existence of further structures in the K^+K^- system.

5 A model of $q\bar{q}$ bound states

Nonrelativistic quark potential models have been applied successfully to heavy quark systems. Such models rely on a Coulomb-plus-linear potential expected from QCD. The extension to the strangeness and light quark (u,d) sectors, however, necessitates the in-

clusion of relativistic effects. A unified framework for light and heavy mesons has been presented in Ref. [6]. This framework relies on a relativistic potential which includes a confining part, a spin-orbit interaction term, a hyperfine interaction term and an annihilation term. The meson spectrum is derived by calculating the bound states in this relativistic potential, and is given in spectroscopic notation $n^{2S+1}L_J$, with n the radial quantum number, S the spin, L the orbital angular momentum and J the total angular momentum.

$n^{2S+1}L_J$	mass	PDG	J^{PC}	mass (PDG)	width (PDG)
1^3S_1	1020	ϕ	1^{--}	1019	4
1^3P_2	1530	f_2' (1525)	2^{++}	1518	86
1^3D_3	1900	ϕ_3	3^{--}	1854	87
1^3F_4	2200	??	??	??	??

Table 2: Mass and width (in MeV) of isoscalar states with hidden strangeness.

In Table 2, the orbital excitations of isoscalar states with hidden strangeness are listed. The 1st and 2nd columns characterize the bound states in spectroscopic notation and give the bound state mass as calculated in Ref. [6]. The 3rd and 4th columns list the associated Particle Data Group (PDG) resonance name, and specify the J^{PC} quantum numbers. Columns 5 and 6 list the PDG resonance mass and width, respectively. The PDG does not list any state which could be associated with the F-wave state as predicted by Ref. [6].

6 Non-linear complex Regge trajectory

The small but existing non-linear dependence of the total angular momentum of a resonance as a function of its mass squared can be used to define a Regge trajectory $\alpha(M^2)$, a complex entity with real and imaginary parts being related by a dispersion relation [7]. In a simple model, the imaginary part is chosen as a sum of single threshold terms,

$$\Im m \alpha(s) = \sum_n c_n (s - s_n)^{1/2} \left(\frac{s - s_n}{s} \right)^{|\Re \alpha(s_n)|} \theta(s - s_n). \quad (1)$$

In Eq. 1, the coefficients c_n are fit parameters, the parameters s_n represent kinematical thresholds of decay channels, and s denotes the centre-of-mass energy [8].

The real part is defined by the value of the total angular momentum, whereas the imaginary part is related to the decay width Γ ,

$$\Im m \alpha(M_R^2) = \Gamma(M_R) \alpha'(M_R) M_R. \quad (2)$$

In Eq. 2, the relation between the imaginary part $\Im m \alpha(M^2)$ and the width function $\Gamma(M)$ of the trajectory is shown, with $\alpha'(M)$ denoting the derivative of the real part.

6.1 The (ϕ, f'_2) -trajectory

A fit to the isoscalar states ϕ, f'_2, ϕ_3 shown in Table 2 defines the (ϕ, f'_2) -trajectory. For the fit, the PDG values for the masses and widths of ϕ, f'_2, ϕ_3 resonances are used.

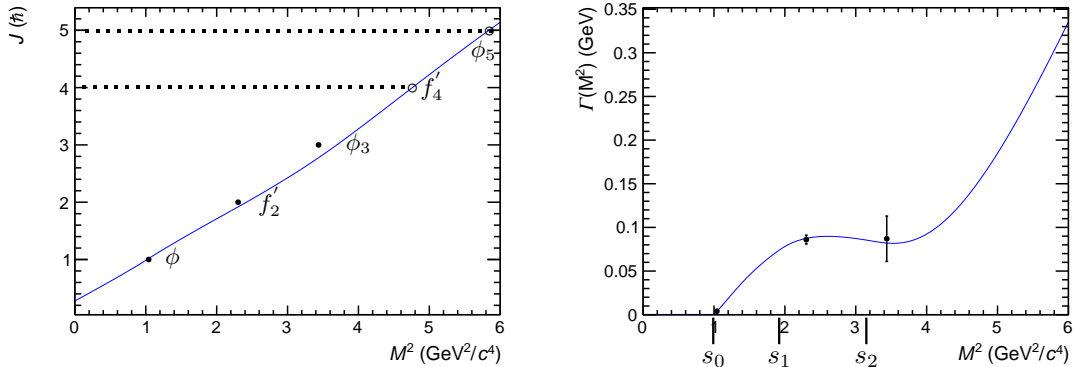


Figure 3: The fit of the (ϕ, f'_2) -trajectory.

In Fig. 3, the fit to the real part of the (ϕ, f'_2) -trajectory is shown on the left, and the fit to the width function $\Gamma(M^2)$ on the right. The thresholds used in this fit are defined by the decays $\phi \rightarrow K\bar{K}$ with $s_0 = 0.97 \text{ GeV}^2$, $f'_2(1525) \rightarrow K\bar{K}^*$ with $s_1 = 1.92 \text{ GeV}^2$ and $\phi_3 \rightarrow K^*\bar{K}^*$ with $s_2 = 3.18 \text{ GeV}^2$. This fit predicts the existence of a f'_4 state with mass of $2182 \text{ MeV}/c^2$ and width of 156 MeV , and of a ϕ_5 state with mass of $2417 \text{ MeV}/c^2$ and width of 310 MeV .

7 Conclusions and outlook

The upgrade of the ALICE detector systems during the shutdown 2019-2021 has resulted in a hundredfold increase of data rate capability. A first analysis of strangeness in double gap events in proton-proton collisions shows clear evidence for the strangeonia states $\phi(1020)$ and $f'_2(1525)$. The data sample taken by ALICE in 2022-2023 is about a factor of 80 larger than the data sample used in the present analysis. This much larger sample will allow the search for two not yet experimentally identified strangeonia states, the $f'_4(2182)$ and the $\phi_5(2417)$. The analysis presented here can be extended to the study of πK pairs, which allows access to the $(u, d)\bar{s}$ kaonium and the $(\bar{u}, \bar{d})s$ antikaonium sector.

8 ACKNOWLEDGMENTS

This work is supported by the German Federal Ministry of Education and Research under promotional reference 05P21VHCA1.

References

- [1] The ALICE coll., ALICE upgrade physics performance studies, ALICE-PUBLIC-2019-001, 2019.
- [2] The ALICE coll., Technical Design Report for the Upgrade of the ALICE Time Projection Chamber, CERN-LHCC-2013-020.
- [3] F. Reidt, Upgrade of the ALICE ITS detector, Nucl.Instrum.Meth.A 1032 (2022) 166632.
- [4] M. Slupecki, Fast Interaction Trigger for ALICE upgrade, Nucl.Instrum.Meth.A 1039 (2022) 167021.
- [5] P. Konopka, B. von Haller, The ALICE O² data quality control system, EPJ Web of Conferences 245, 01027 (2020).
- [6] N. Isgur, S. Godfrey, Mesons in a Relativized Quark Model with Chromodynamics, Phys. Rev.D32, 189, 1985.
- [7] A.I. Bugrij et al., Fortschr. Phys., 21, (1973) 427.
- [8] R. Schicker, Acta Phys. Pol. B Proc. Suppl. 16, 5-A9 (2023).